Letter | Editors' Suggestion

Intertwined magnetism and superconductivity in isolated correlated flat bands

Xuepeng Wang,[1] J. F. Mendez-Valderrama,[1] Johannes S. Hofmann,[2,3,*] and Debanjan Chowdhury[1,†]
[1]*Department of Physics, Cornell University, Ithaca, New York 14853, USA*
[2]*Department of Condensed Matter Physics, Weizmann Institute of Science, Rehovot 76100, Israel*
[3]*Max-Planck-Institut für Physik komplexer Systeme, Nöthnitzer Strasse 38, 01187 Dresden, Germany*

(Received 18 February 2024; revised 10 June 2024; accepted 12 June 2024; published 1 July 2024)

Multiorbital electronic models hosting a nontrivial band topology in the regime of strong electronic interactions are an ideal playground for exploring a host of complex phenomenology. We consider here a sign-problem-free and time-reversal symmetric model with isolated topological (Chern) bands involving both spin and valley degrees of freedom in the presence of a class of repulsive electronic interactions. Using a combination of numerically exact quantum Monte Carlo computations and analytical field-theoretic considerations, we analyze the phase diagram as a function of the flat-band filling, temperature, and relative interaction strength. The low-energy physics is described in terms of a set of intertwined orders—a spin-valley Hall (SVH) insulator and a spin-singlet superconductor (SC). Our low-temperature phase diagram can be understood in terms of an effective SO(4) pseudospin nonlinear sigma model. Our work paves the way for building more refined and minimal models of realistic materials, including moiré systems, to study the universal aspects of competing insulating phases and superconductivity in the presence of nontrivial band topology.

DOI: 10.1103/PhysRevB.110.L041105

Introduction. Correlated quantum materials in the intermediate to strong coupling regime often feature a panoply of ordering tendencies leading to complex phase diagrams. The most famous and extensively studied example is that of the cuprate high-temperature superconductor—a doped Mott insulator which exhibits numerous electronic phases with spontaneously broken symmetries as a result of the frustration between the tendency toward delocalization and the interaction-induced localization [1]. While the detailed microscopic mechanisms responsible for the emergence of this complexity are not fully understood, the landscape of competing and intertwined orders has been clarified to a large degree using a variety of points of view [2–6].

The discovery of two-dimensional moiré materials [7,8] has brought a fresh set of challenging theoretical questions to the forefront, involving the physics of interactions projected to a set of isolated nearly flat bands. The projected interactions drive the tendency toward delocalization, as a result of the nontrivial Bloch wave functions associated with the flat bands, and localization in the vicinity of commensurate fillings. The quantum geometric tensor associated with these isolated bands is believed to play an important role in much of the essential phenomenology [9–11]. In the absence of a well-developed set of theoretical tools and a "small" parameter that can tackle the generic problem of partially filled, interacting narrow bandwidth (topological) bands, studying even simplified models with carefully designed interactions using complementary techniques can offer new insights and serve as a building block for understanding more realistic models. Specifically, the fate of nearly flat bands with multiple spin and valley degrees of freedom and projected interactions offers an interesting playground to study the interplay of various ordering tendencies, including superconductivity.

With this goal in mind, we will focus on a model of spinful topological (Chern) bands that preserve time-reversal symmetry (TRS) and carry a "valley" degree of freedom. We will study the effect of competing exchange interactions derived, in principle, from a repulsive interaction but designed such that the model does *not* suffer from the infamous sign problem. This will allow us to obtain the phase diagram for the repulsive model over a wide range of temperatures, fillings, and other microscopic tuning parameters using determinant quantum Monte Carlo (QMC), whereas most of the recent QMC work tied to flat bands has focused on purely attractive interactions [12–16]. Interestingly, we will also be able to obtain the form of the low-energy effective field theory that governs the dynamics and fluctuations tied to the intertwined order parameters in the projected Hilbert space, offering complementary analytical insights into the same problem.

Model. We consider a two-dimensional interacting model of topological bands with Chern number, $C = \pm 1$, that preserves TRS. The noninteracting bands are obtained microscopically in a model of electrons hopping on the sites of a square lattice [12,17], where the degrees of freedom consist of spin ($\sigma = \uparrow, \downarrow$), valley ($\tau = \pm$), and sublattice ($\eta =$ A, B), respectively. The noninteracting part of the Hamiltonian per spin $H_{\rm kin}^{(\sigma)}$ can be written in momentum space as [12]

$$H_{\rm kin}^{(\sigma)} = \sum_{\boldsymbol{k}} \psi_{\boldsymbol{k}}^{\dagger}[B_{0,\boldsymbol{k},\sigma}\eta_0 + \boldsymbol{B}_{\boldsymbol{k},\boldsymbol{\sigma}} \cdot \boldsymbol{\eta}]\tau_0\psi_{\boldsymbol{k}}, \tag{1}$$

*Contact author: jhofmann@pks.mpg.de
†Contact author: debanjanchowdhury@cornell.edu

where $\psi_{\boldsymbol{k}}^{\dagger} = (f_{\boldsymbol{k},A,+}^{\dagger}, f_{\boldsymbol{k},B,+}^{\dagger}, f_{\boldsymbol{k},A,-}^{\dagger}, f_{\boldsymbol{k},B,-}^{\dagger})$ and $f_{\boldsymbol{k},\eta,\tau}^{\dagger}$ denotes the electron creation operator on sublattice η with valley τ. Here, $B_{0,\boldsymbol{k},\sigma}$ and $\boldsymbol{B}_{\boldsymbol{k},\sigma}$ are matrices determined entirely by the hopping parameters on the underlying lattice, which we assume to include first (t) and staggered second ($t_2 = t/\sqrt{2}$) neighbor hoppings with a π flux per square plaquette [18]. Additionally, by including further (e.g., fifth t_5) neighbor hoppings, the flatness ratio $\mathcal{F} = W/E_{\rm gap}$ ($W \equiv$ bandwidth, $E_{\rm gap} \equiv$ band gap) can be tuned to be small. By including two copies of $H_{\rm kin}^{(\sigma)}$ in a time-invariant fashion [18], under the operation $\mathcal{T} = i\sigma_y\mathcal{K}$ where $\mathcal{K}$ denotes complex conjugation, we arrive at a model with a set of degenerate topological bands carrying spin and valley with $C = \sigma$. Note that the noninteracting part of the Hamiltonian has a $\mathrm{SU}(2)_{\rm valley} \times \mathrm{U}(1)_{\rm spin} \times \mathrm{U}(1)_{\rm c}$ symmetry, which is broken *explicitly* down to $\mathrm{U}(1)_{\rm valley} \times \mathrm{U}(1)_{\rm spin} \times \mathrm{U}(1)_{\rm c}$ by the interaction we introduce below.

Our choice of interactions will be inspired by the physics of quantum Hall-type ferromagnetism in spinful Landau levels [19–22]. We will focus on the competing effects of an intravalley Hund's-type ferromagnetic interaction with $J_{\rm H} < 0$, and an intervalley antiferromagnetic interaction with $J_{\rm A} > 0$, and study the competition between possible valley symmetry-breaking phases and superconductivity in a model with two time-reversed Chern sectors, as introduced above. The interactions take the following form:

$$H_{\rm interaction} = H_{\rm intravalley} + H_{\rm intervalley}, \tag{2a}$$

$$H_{\rm intravalley} = J_{\rm H} \sum_{\mathbf{r},\tau=\pm} \boldsymbol{S}_{\mathbf{r}}^{\tau} \cdot \boldsymbol{S}_{\mathbf{r}}^{\tau}, \tag{2b}$$

$$H_{\rm intervalley} = J_{\rm A} \sum_{\boldsymbol{r}} \boldsymbol{S}_{\mathbf{r}}^{+} \cdot \boldsymbol{S}_{\mathbf{r}}^{-}, \tag{2c}$$

where the "spin" operator is defined as

$$\boldsymbol{S}_{\mathbf{r}}^{\tau} = \sum_{\alpha,\beta=\uparrow,\downarrow} f_{\mathbf{r},\tau,\alpha}^{\dagger} \boldsymbol{\sigma}_{\alpha\beta} f_{\mathbf{r},\tau,\beta}. \tag{3}$$

We have combined the two-dimensional spatial coordinate and the sublattice index (η) into $\mathbf{r}$. Note that we have only included an on-site interaction in the full microscopic Hamiltonian (which generates further-neighbor interactions upon projection to the lower flat bands).

Quantum Monte Carlo. The model introduced above possesses an antiunitary TRS, $\mathcal{T}' = i\tau_x\sigma_y\mathcal{K}$, which enables a sign-problem-free quantum Monte Carlo computation at arbitrary filling fraction ν [18,23] as long as $J_{\rm A} \geqslant 2|J_{\rm H}|$. The partition function for the model defined by Eqs. (1) and (2) is evaluated using a Trotter decomposition with $\Delta\tau = \beta/N_{\rm Trotter}$, where the interaction is factorized via a discrete Hubbard-Stratonovich transformation and the auxiliary fields are sampled stochastically using single spin-flip updates [18]. In the remainder of this manuscript, we will primarily focus on the problem with $J_{\rm A} = 2|J_{\rm H}|$; this parameter choice corresponds to maximizing the contribution due to Hund's interaction relative to the antiferromagnetic exchange, where Hund's coupling is expected to be naturally induced from an on-site intravalley Hubbard repulsion. To address the relative importance of the bare band dispersion vs (projected) interactions, we will present results for a flatness ratio, $\mathcal{F} = 0.009$, 0.2, and $J_{\rm A}/t = 2.5 - 5$; the gap to the remote

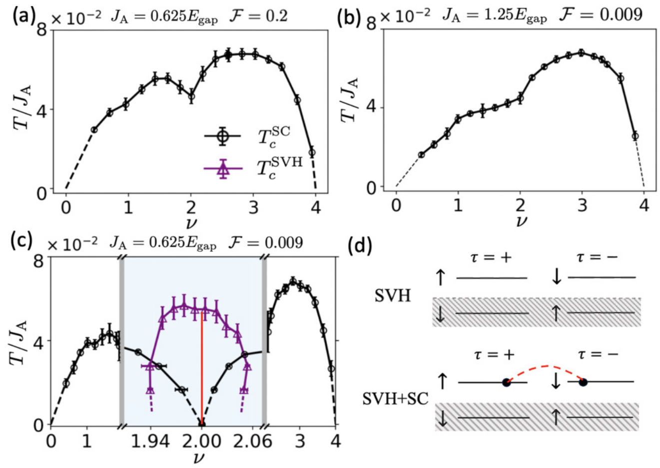

FIG. 1. Superconducting phase diagrams for $|J_{\rm H}| = J_{\rm A}/2$ with (a) $J_{\rm A}/t = 2.5$ and $\mathcal{F} = 0.2$, showing a slight suppression of the superconducting $T_c^{\rm SC}$ near $\nu = 2$; (b) $J_{\rm A}/t = 5$ and $\mathcal{F} = 0.009$; and (c) $J_{\rm A}/t = 2.5$ and $\mathcal{F} = 0.009$, where the zoomed-in blue-shaded region shows the competing SVH insulating state (red solid line) near $\nu = 2$. The lightly doped regions near $\nu = 2$ exhibit a regime with coexisting SC and SVH order for $T < \min(T_c^{\rm SC}, T_c^{\rm SVH})$; see Fig. 2. (d) The top panel shows a schematic of the SVH insulator at $\nu = 2$ with the shaded regions denoting fully filled electronic bands. The bottom panel is a schematic for the coexisting SVH and SC phases for $\nu = 2 + \delta\nu$, where the excess electrons (black circles) form spin-singlet Cooper pairs (red dashed line).

bands, $E_{\rm gap} \simeq 4t$. To obtain the phase diagram as a function of temperature and band filling, we tune the chemical potential $\mu(T)$ such that $\sum_{\mathbf{r}} \langle n_{\mathbf{r}} \rangle / L^2 = \nu$, where ν denotes the filling of the Chern bands and $n_{\mathbf{r}} = \sum_{\tau,\sigma} f_{\mathbf{r},\tau,\sigma}^{\dagger} f_{\mathbf{r},\tau,\sigma}$ is the local electron density ($L^2 \equiv$ system size).

Superconductivity and intertwined orders. Let us begin by discussing the results for the model with $\mathcal{F} = 0.2$ ($t_5 = 0$) and $J_{\rm A}/t = 2.5$; the bands have some dispersion but the interaction scale is small compared to $E_{\rm gap}$. We find the ground state to be a superconductor over the entire range of fillings, and the transition temperature ($T_c^{\rm SC}$) vanishes when $\nu \to 0^+, 4^-$ [see Fig. 1(a)]. We compute the temperature-dependent superfluid stiffness $D_s(T)$ as the transverse electromagnetic response at vanishing Matsubara frequency [24],

$$D_s = \tfrac{1}{4} \langle [-K_{xx} - \Lambda_{xx}(\omega_n = 0, q_y = 0, q_x \to 0)] \rangle, \tag{4}$$

where $\Lambda_{xx}(\omega_n, \boldsymbol{q})$ is paramagnetic current-current correlation, and $K_{xx} \equiv \langle \partial^2 H[\boldsymbol{A}]/\partial A_x^2|_{\boldsymbol{A}\to 0} \rangle$ is the diamagnetic contribution, with $\boldsymbol{A}$ the probe vector potential. The superconducting transition temperature $T_c^{\rm SC}$ is then determined as $T_c^{\rm SC} = \pi D_s(T \to T_c^{\rm SC-})/2$ [25].

Interestingly, we notice a clear suppression of $T_c^{\rm SC}$ near $\nu = 2$. To compute the tendencies toward pairing and other orders, we introduce the thermodynamic susceptibilities for an observable O,

$$\chi_O = \frac{1}{L^2} \int d\tau \langle O^{\dagger}(\tau) O(\tau = 0) \rangle. \tag{5}$$

The first observable of interest is associated with a spin-singlet, on-site s-wave pairing operator,

$$\Delta^\dagger_{\mathrm{SC}} \equiv \sum_{\mathbf{r}} [c^\dagger_{\mathbf{r},+\uparrow} c^\dagger_{\mathbf{r},-\downarrow} - c^\dagger_{\mathbf{r},+\downarrow} c^\dagger_{\mathbf{r},-\uparrow}], \tag{6}$$

which also pairs across valleys. The other operator of interest diagnoses the tendency toward an intravalley ferromagnetic polarization ($\propto [n_{\tau\uparrow} - n_{\tau\downarrow}]$, $\tau = \pm$) and an intervalley antiferromagnetic order ($\propto [n_{+\uparrow} + n_{-\downarrow}]$). We define the associated spin-valley Hall (SVH) order parameter as

$$\Delta_{\mathrm{SVH}} \equiv \sum_{\mathbf{r}} [n_{\mathbf{r},+\uparrow} + n_{\mathbf{r},-\downarrow} - n_{\mathbf{r},+\downarrow} - n_{\mathbf{r},-\uparrow}]. \tag{7}$$

Note that if this observable develops an expectation value near $\nu = 2$, it preserves the global TRS. For the data in Fig. 1(a), we have computed the spin-valley Hall susceptibility, and a finite-size scaling suggests that the system fails to develop this competing order even though T_c^{SC} undergoes a downward renormalization (presumably due to enhanced SVH fluctuations) [18]. This is our first indication that SC and SVH orders are intertwined in this model, but depending on values of microscopic parameters, one of the two orders becomes energetically favorable.

To investigate further the possibility of enhancing the tendency to form an insulating ground state at the commensurate filling of $\nu = 2$, we focus next on a much flatter band with $\mathcal{F} = 0.009$ [$t_5 = (1 - \sqrt{2})t/4$] and two different values of the interaction. For $J_{\mathrm{A}}/t = 5$, the suppression of T_c^{SC} near $\nu = 2$ disappears, and the ground state remains a superconductor for all fillings [Fig. 1(b)]. In spite of the bands being much flatter, it is worth noting that $J_{\mathrm{A}} = 5t \gtrsim E_{\mathrm{gap}}$, leading to a mixing with the degrees of freedom from the dispersive remote bands. The model is no longer in the "projection-only" limit, leading to a reduction in the associated strong-coupling effect tied to just the flat-band Hilbert space [18].

Finally, keeping $\mathcal{F} = 0.009$ and decreasing the interaction strength to $J_{\mathrm{A}} = 2.5t < E_{\mathrm{gap}}$, we find a complete suppression of $T_c^{\mathrm{SC}} \to 0$ at $\nu = 2$ [Fig. 1(c)]. Using finite-size scaling for χ_{SC} and χ_{SVH}, and by carrying out a $T = 0$ projective QMC calculation, we provide unambiguous evidence for the ground state being an interaction-induced SVH insulator [18]; see vertical orange line in Fig. 1(c). This indicates that effectively projecting to only the degrees of freedom in the lower "flatter" bands enhances the commensuration effects at integer filling, in contrast to the previous two cases. We turn next to studying the effect of doping carriers away from the $\nu = 2$ insulator on the many-body phase diagram; see Fig. 1(d).

It is worth noting that while the $\nu = 2$ insulator is incompressible, any doping away from this limit will lead to a compressible phase. Moreover, given the prevalence of superconductivity in the model in the absence of the insulating regime, it is likely that the doped model displays superconducting correlations. Thus, the following scenarios for the phase diagram are possible when $\nu = 2 \pm \delta\nu$: (1) a first-order transition between the SVH insulator and superconductivity at infinitesimal $\delta\nu$, (2) phase separation between the SVH insulator and SC over a range of intermediate $\delta\nu$, and (3) a phase with microscopically coexistent SVH order and SC. To diagnose the competition between SVH and SC phases, we focus on the renormalization group (RG)-invariant correlation

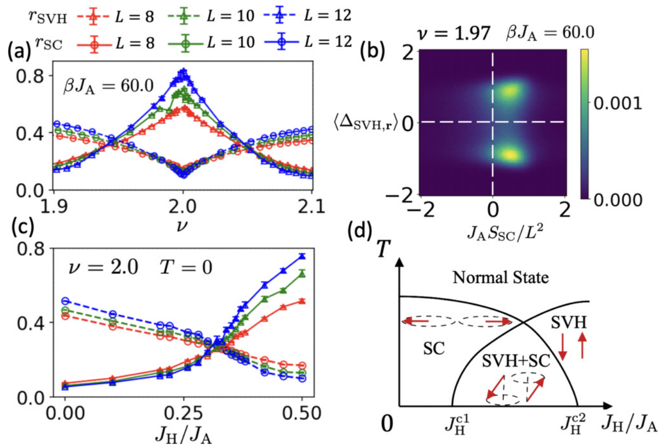

FIG. 2. (a) RG-invariant correlation lengths r_{SVH} (solid line) and r_{SC} (dashed line) as a function of ν at $\beta J_{\mathrm{A}} = 60$ for $J_{\mathrm{A}}/t = 2.5$ and $\mathcal{F} = 0.009$ with $|J_{\mathrm{H}}| = J_{\mathrm{A}}/2$. For both hole and electron doping relative to $\nu = 2$, there exists a regime where both SC and SVH phases coexist for $\nu_c^{\mathrm{SC}} < \nu < \nu_c^{\mathrm{SVH}}$. (b) Histogram of SVH order parameter $\langle \Delta_{\mathrm{SVH}} \rangle$ and equal-time correlation function $S_{\mathrm{SC}}(\boldsymbol{q} = 0)$ measured *per Monte Carlo snapshot* for $\nu = 1.97$ and $\beta J_{\mathrm{A}} = 60$ indicates their microscopic coexistence. (c) The same RG-invariant correlation lengths as a function of $J_{\mathrm{H}}/J_{\mathrm{A}}$ at $\nu = 2$ and $T = 0$. There exists a regime of microscopic coexistence of SC and SVH phases for $J_{\mathrm{H}}^{c1} < J_{\mathrm{H}} < J_{\mathrm{H}}^{c2}$. (d) A schematic T-J_{H} phase diagram expressed using the pseudospin effective model [26].

length r_O obtained from the equal-time correlation function $S_O(\boldsymbol{q})$ as

$$r_O \equiv \frac{\xi_O}{L} = \frac{1}{2L\sin(\pi/L)} \sqrt{\frac{S_O(\boldsymbol{q} = \mathbf{0})}{S_O[\boldsymbol{q} = (2\pi/L, 0)]} - 1}, \tag{8a}$$

$$S_O(\boldsymbol{q}) = \frac{1}{L^2} \sum_{\mathbf{r},\mathbf{r}'} e^{-i(\mathbf{r}-\mathbf{r}')\cdot\boldsymbol{q}} \langle O^\dagger(\mathbf{r}') O(\mathbf{r}) \rangle. \tag{8b}$$

By extracting T_c^{SVH} (purple triangles) and T_c^{SC} (black circles) in Fig. 1(c) at a fixed filling in the vicinity of $\nu = 2$, we find that both orders are present below $T < \min(T_c^{\mathrm{SVH}}, T_c^{\mathrm{SC}})$. We note that the slight "bending" of T_c^{SVH} with decreasing temperature inside the superconducting phase is likely due to the competition between the two orders.

We have analyzed the correlation length for SVH and SC as a function of filling fraction ν at a fixed temperature $\beta J_{\mathrm{A}} = 60.0$, as shown in Fig. 2(a). Our finite size scaling analysis suggests that there exists a range of $\delta\nu$ on either side of $\nu = 2$, where SVH order survives and $T_c^{\mathrm{SC}} \propto |\delta\nu|$.

To address the question of microscopic coexistence vs phase separation, we analyze the histogram of SVH order parameter $\langle \Delta_{\mathrm{SVH}} \rangle$ and equal-time correlation function $S_{\mathrm{SC}}(\boldsymbol{q} = 0)$ measured *per Monte Carlo snapshot*, instead of ensemble-averaged observables. The histogram for $\nu = 1.97$ and $\beta J_{\mathrm{A}} = 60$ is shown in Fig. 2(b). If the system had a tendency to phase separate, the Monte Carlo snapshots would show *either* SVH *or* SC order, appearing as "blobs" along the axes in the histogram. One the other hand, an off-diagonal peak of the histogram in Fig. 2(b) suggests that within each Monte Carlo snapshot, both SVH and SC orders coexist, indicating a coexistence between SVH and SC orders for $\nu = 1.97$ and $\beta J_{\rm A} = 60$.

Instead of tuning the filling near $\nu = 2$ at a fixed value of $|J_{\rm H}|/J_{\rm A}$ and driving transitions between the different phases, we can gain complementary insights into the strong-coupling limit by varying the ratio of interactions at a fixed $\nu = 2$. A finite-size scaling analysis [27] of the correlation length ratios obtained from our $T = 0$ projective simulations are shown in Fig. 2(c). At $\nu = 2$ we find a coexistence of SVH and SC orders between $|J_{\rm H}^{c1}|/J_{\rm A} = 0.295(3)$ and $|J_{\rm H}^{c2}|/J_{\rm A} = 0.342(4)$. To help unify our understanding of these competing phases and their phase transitions, let us turn next to an analytical approach that helps tie together the numerical phenomenology.

Analytical results. Given the orders we found in our QMC computations, it is natural to address the nature of the effective field theory for a "superspin" [28–30] that describes the phases and possible phase transitions in the low-energy Hilbert space; such approaches have been used earlier in the context of orders in the cuprates [31–34]. We introduce the Nambu spinors, $\Psi^\dagger \equiv (c_{+\uparrow}^\dagger, c_{-\uparrow}^\dagger, c_{+\downarrow}, c_{-\downarrow})$, and the Pauli matrices μ_α which act on the particle-hole subspace. The three-dimensional pseudospin vector operator, $\boldsymbol{n} \equiv (\mathrm{Re}[\Delta_{\rm SC}], -\mathrm{Im}[\Delta_{\rm SC}], \Delta_{\rm SVH})$, encodes the competing orders of interest and can be expressed as bilinears of Ψ:

$$\begin{aligned} n_1 &= \tfrac{1}{2}\Psi^\dagger \mu_x \tau_x \Psi \equiv \mathrm{Re}[\Delta_{\rm SC}], \\ n_2 &= \tfrac{1}{2}\Psi^\dagger \mu_y \tau_x \Psi \equiv -\mathrm{Im}[\Delta_{\rm SC}], \\ n_3 &= \tfrac{1}{2}\Psi^\dagger \tau_z \Psi \equiv \Delta_{\rm SVH}. \end{aligned} \tag{9}$$

Naively, one might expect the low-energy theory to be described purely in terms of $\boldsymbol{n}$, until one notices that these sets of operators do not form a closed group. The minimal group that contains the $\{n_\alpha, \alpha = 1, 2, 3\}$ as generators is SO(4). The remaining three generators $\{L_\alpha\}$ act as the angular momentum of n_α and are given by

$$\begin{aligned} L_1 &= -\frac{1}{2}\Psi^\dagger \mu_y \tau_y \Psi \equiv \mathrm{Re}[\Delta_{\rm vSC}], \\ L_2 &= \frac{1}{2}\Psi^\dagger \mu_x \tau_y \Psi \equiv -\mathrm{Im}[\Delta_{\rm vSC}], \\ L_3 &= \frac{1}{2}\Psi^\dagger \mu_z \Psi = \frac{1}{2}\Big(\sum_{\tau,\sigma} n_{\tau,\sigma} - 2\Big), \end{aligned} \tag{10}$$

where the additional order parameter is

$$\Delta_{\mathbf{r},{\rm vSC}} \equiv [c_{\mathbf{r},-\downarrow}c_{\mathbf{r},+\uparrow} + c_{\mathbf{r},-\uparrow}c_{\mathbf{r},+\downarrow}]. \tag{11}$$

The above pseudospin operators can be mapped to the spin operators on a bipartite lattice [26,35] where the L_α represent the uniform magnetization, while the n_α are equivalent to the staggered magnetization in the α direction of the spin model, respectively [18].

Projecting the interactions in Eq. (2) to the lower flat bands, we obtain the following low-energy effective Hamiltonian:

$$\begin{aligned} \mathcal{H}_{\rm eff} &= \sum_{\mathbf{r},\alpha}\big[G\big(U_\alpha L_{\alpha,\mathbf{r}}^2 + V_\alpha n_{\alpha,\mathbf{r}}^2\big) + \mu L_{3,\mathbf{r}}\big] \\ &\quad + \sum_{\mathbf{r},\mathbf{r}',\alpha} F_{\mathbf{r},\mathbf{r}'}\big[U_\alpha' L_{\alpha,\mathbf{r}}L_{\alpha,\mathbf{r}'} + V_\alpha' n_{\alpha,\mathbf{r}}n_{\alpha,\mathbf{r}'}\big], \end{aligned} \tag{12}$$

where the coefficients are given by

$$U_1 = U_2 = \frac{J_A}{5} + \frac{3|J_H|}{10}, \quad U_3 = -\frac{J_A}{20} + \frac{3|J_H|}{10} \tag{13a}$$

$$V_1 = V_2 = -\frac{3J_A}{10} + \frac{3|J_H|}{10}, \quad V_3 = -\frac{3J_A}{10} - \frac{6|J_H|}{5} \tag{13b}$$

$$U_1' = U_2' = \frac{J_A}{8}, \quad U_3' = \frac{3|J_H|}{4} \tag{13c}$$

$$V_1' = V_2' = -\frac{3J_A}{8}, \quad V_3' = -\frac{J_A}{4} - \frac{3|J_H|}{4}. \tag{13d}$$

Here, μ acts as a pseudo magnetic field. Note that the model does not have any (emergent) SO(4) symmetry, but it nevertheless provides an organizing framework to describe the various order-parameter fluctuations. The coefficients G and $F_{\mathbf{r},\mathbf{r}'}$ are positive and can be obtained in terms of the Wannier functions constructed out of the lower flat-band Bloch wave functions; their precise form is unimportant for describing the phases and phase transitions at $T = 0$, which we turn to next.

When $\mu = 0$, the effective Hamiltonian in Eq. (12) hosts an anisotropy-tuned easy axis to easy-plane transition with decreasing $|J_{\rm H}|/J_{\rm A}$, as seen in our numerical data in Fig. 2(c). The pseudospin-flop transition has been studied theoretically in classic papers [26,35]; a schematic phase diagram as a function of $J_{\rm H}/J_{\rm A}$ and T appears in Fig. 2(d). Let us now elaborate further on the connections between the pseudospin model and the numerically obtained phase diagram at $T = 0$. For $\nu = 2$, the uniform polarization $\langle L_3\rangle = 0$ vanishes across the entire phase diagram. When $J_{\rm H}/J_{\rm A} = 0$, the competition between the isotropic on-site term and the long-range interactions generated by $F_{\mathbf{r},\mathbf{r}'}$ lead to an easy-plane Neel state with $\langle n_{1,2}\rangle \neq 0$, suggesting that the ground state is a spin-singlet superconductor [Fig. 2(d)].

The gapped SC ground state remains stable with increasing $|J_{\rm H}| < |J_{\rm H}^{c1}|$, across which there appears a continuous quantum phase transition to a phase with coexisting SVH and SC orders. In the pseudospin language, for $|J_{\rm H}^{c1}| < |J_{\rm H}| < |J_{\rm H}^{c2}|$, they tilt away from the xy plane, such that both the SC order parameter $\langle n_{1,2}\rangle \neq 0$ and SVH order parameter $\langle n_3\rangle \neq 0$. Increasing $|J_{\rm H}|$ beyond $|J_{\rm H}^{c2}|$ turns the easy-plane anisotropy in Eq. (12) to an easy-axis anisotropy, where SC disappears ($\langle n_{1,2}\rangle = 0$) and only the SVH order parameter survives $\langle n_3\rangle \neq 0$. The chemical potential tuned transitions between the SVH and SC phases can also be described within the above picture in terms of an external magnetic-field-tuned pseudospin-flop transition [26,35]; see Ref. [18] for a detailed discussion of the differences from the present case.

To finally address the universality class associated with the distinct anisotropy-tuned phase transitions [26,35] for $T = 0$ and $\nu = 2$ at $J_{\rm H}^{c1}$ and $J_{\rm H}^{c2}$, we perform a scaling collapse analysis in Fig. 3. The onset of SVH order in the presence of a background SC order at $J_{\rm H} = J_{\rm H}^{c1}$ (where the fermions are already gapped) belongs in the (2 + 1)-dimensional Ising universality class; the correlation-length critical exponent in Fig. 3(a) is consistent with Ising criticality. Similarly, the loss of SC at $J_{\rm H} = J_{\rm H}^{c2}$ in the absence of any gapless fermions belongs in the (2 + 1)-dimensional XY universality class, as can be seen from the rescaled data in Fig. 3(b).

Outlook. We have studied the effects of competing intravalley ferromagnetic and intervalley antiferromagnetic

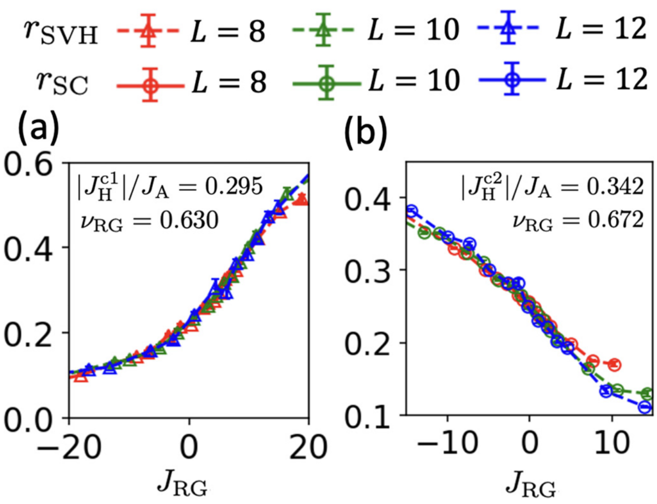

FIG. 3. Scaling collapse analysis of the anisotropy-tuned transition at $T=0$ and $\nu=2.0$ for (a) the onset of SVH order, described by a $(2+1)$-dimensional Ising theory, and (b) the loss of SC order, associated with a $(2+1)$-dimensional XY transition. The RG invariant tuning parameter is defined as $J_{\rm RG}=[(J_{\rm H}-J_{\rm H}^{\rm c})/J_{\rm H}^{\rm c}]L^{1/\nu_{\rm RG}}$, with $J_{\rm H}^{\rm c}$ labeled in the respective panels.

interactions—derived from a purely repulsive electronic interaction—projected to a set of isolated topological flat bands. The low-energy physics is described by a set of intertwined orders involving a spin-valley Hall insulator and superconductor near the commensurate filling of $\nu=2$. Clearly, this competition also rules out the prospect of any applicable *lower* bounds on the superconducting $T_c^{\rm SC}$ [15], in contrast with analogous suggestions for models with onsite attractive interactions [16,36,37]. In the symmetry-broken phases, we have also identified the effective field theory for the intertwined orders, and pinned down the universal theories for the associated phase transitions. The universal physics near the finite-temperature multicritical point deserves a more careful study in the future, as the normal metallic phase without any symmetry-breaking orders involves gapless fermions coupled to the critical order-parameter fluctuations.

Our findings have a number of conceptual similarities with the phenomenology of correlated insulators and superconductivity, when doped away from the commensurate fillings, in moiré graphene. A recent moiré-inspired numerical study has also highlighted the role of competing orders for models of topological multiorbital flat bands with the full repulsive density-density interactions [38]. It has not escaped our attention that our model shares superficial similarities with a model displaying skyrmion mediated pairing as well [28–30]. However, our current model does not yield skyrmionic excitations within a Chern sector as the cheapest excitation. Other variations of the above model may be able to host a quantum Hall-like ferromagnetic ground state at integer filling and possibly a skyrmion-mediated superconducting phase, which we leave for future study. In addition, investigating various proxies for electrical transport near the symmetry-breaking transitions remains an exciting avenue.

The auxiliary field QMC simulations were carried out using the ALF package [39].

Acknowledgments. We thank Erez Berg for a number of interesting discussions and related collaborations. J.H. was supported by the European Research Council (ERC) under grant HQMAT (Grant No. 817799), the US-Israel Binational Science Foundation (BSF), and a research grant from Irving and Cherna Moskowitz. This work is supported in part by a Sloan research fellowship from the Alfred P. Sloan foundation to D.C. This work used Expanse at the San Diego Supercomputer Center through allocation TG-PHY210006 from the Advanced Cyberinfrastructure Coordination Ecosystem: Services & Support (ACCESS) program [40], which is supported by National Science Foundation Grants No. 2138259, No. 2138286, No. 2138307, No. 2137603, and No. 2138296.

[1] B. Keimer, S. A. Kivelson, M. R. Norman, S. Uchida, and J. Zaanen, From quantum matter to high-temperature superconductivity in copper oxides, Nature (London) **518**, 179 (2015).
[2] E. Demler, W. Hanke, and S.-C. Zhang, SO(5) theory of antiferromagnetism and superconductivity, Rev. Mod. Phys. **76**, 909 (2004).
[3] S. Sachdev, Colloquium: Order and quantum phase transitions in the cuprate superconductors, Rev. Mod. Phys. **75**, 913 (2003).
[4] P. A. Lee, N. Nagaosa, and X.-G. Wen, Doping a Mott insulator: Physics of high-temperature superconductivity, Rev. Mod. Phys. **78**, 17 (2006).
[5] E. Fradkin, S. A. Kivelson, and J. M. Tranquada, Colloquium: Theory of intertwined orders in high temperature superconductors, Rev. Mod. Phys. **87**, 457 (2015).
[6] D. F. Agterberg, J. S. Davis, S. D. Edkins, E. Fradkin, D. J. Van Harlingen, S. A. Kivelson, P. A. Lee, L. Radzihovsky, J. M. Tranquada, and Y. Wang, The physics of pair-density waves: Cuprate superconductors and beyond, Annu. Rev. Condens. Matter Phys. **11**, 231 (2020).
[7] E. Y. Andrei, D. K. Efetov, P. Jarillo-Herrero, A. H. MacDonald, K. F. Mak, T. Senthil, E. Tutuc, A. Yazdani, and A. F. Young, The marvels of moiré materials, Nat. Rev. Mater. **6**, 201 (2021).
[8] K. F. Mak and J. Shan, Semiconductor moiré materials, Nat. Nanotechnol. **17**, 686 (2022).
[9] P. Törmä, S. Peotta, and B. A. Bernevig, Superconductivity, superfluidity and quantum geometry in twisted multilayer systems, Nat. Rev. Phys. **4**, 528 (2022).
[10] P. J. Ledwith, G. Tarnopolsky, E. Khalaf, and A. Vishwanath, Fractional Chern insulator states in twisted bilayer graphene: An analytical approach, Phys. Rev. Res. **2**, 023237 (2020).
[11] C. Repellin and T. Senthil, Chern bands of twisted bilayer graphene: Fractional Chern insulators and spin phase transition, Phys. Rev. Res. **2**, 023238 (2020).
[12] J. S. Hofmann, E. Berg, and D. Chowdhury, Superconductivity, pseudogap, and phase separation in topological flat bands, Phys. Rev. B **102**, 201112(R) (2020).

[13] V. Peri, Z.-D. Song, B. A. Bernevig, and S. D. Huber, Fragile topology and flat-band superconductivity in the strong-coupling regime, Phys. Rev. Lett. **126**, 027002 (2021).
[14] X. Zhang, K. Sun, H. Li, G. Pan, and Z. Y. Meng, Superconductivity and bosonic fluid emerging from moiré flat bands, Phys. Rev. B **106**, 184517 (2022).
[15] J. S. Hofmann, E. Berg, and D. Chowdhury, Superconductivity, charge density wave, and supersolidity in flat bands with a tunable quantum metric, Phys. Rev. Lett. **130**, 226001 (2023).
[16] J. Herzog-Arbeitman, V. Peri, F. Schindler, S. D. Huber, and B. A. Bernevig, Superfluid weight bounds from symmetry and quantum geometry in flat bands, Phys. Rev. Lett. **128**, 087002 (2022).
[17] T. Neupert, L. Santos, C. Chamon, and C. Mudry, Fractional quantum Hall states at zero magnetic field, Phys. Rev. Lett. **106**, 236804 (2011).
[18] See Supplemental Material at http://link.aps.org/supplemental/10.1103/PhysRevB.110.L041105 for additional details on the numerical procedures and data.
[19] S. M. Girvin, A. H. MacDonald, and P. M. Platzman, Magneto-roton theory of collective excitations in the fractional quantum Hall effect, Phys. Rev. B **33**, 2481 (1986).
[20] S. L. Sondhi, A. Karlhede, S. A. Kivelson, and E. H. Rezayi, Skyrmions and the crossover from the integer to fractional quantum Hall effect at small Zeeman energies, Phys. Rev. B **47**, 16419 (1993).
[21] K. Moon, H. Mori, K. Yang, S. M. Girvin, A. H. MacDonald, L. Zheng, D. Yoshioka, and S.-C. Zhang, Spontaneous interlayer coherence in double-layer quantum Hall systems: Charged vortices and Kosterlitz-Thouless phase transitions, Phys. Rev. B **51**, 5138 (1995).
[22] S. M. Girvin, The quantum Hall effect: Novel excitations and broken symmetries, in *Topological Aspects of Low Dimensional Systems*, edited by A. Comtet, T. Jolicoeur, S. Ouvry, and F. David (Springer-Verlag, Berlin and Les Editions de Physique, Les Ulis, 2000).
[23] C. Wu and S.-C. Zhang, Sufficient condition for absence of the sign problem in the fermionic quantum Monte Carlo algorithm, Phys. Rev. B **71**, 155115 (2005).
[24] D. J. Scalapino, S. R. White, and S. Zhang, Insulator, metal, or superconductor: The criteria, Phys. Rev. B **47**, 7995 (1993).
[25] D. R. Nelson and J. M. Kosterlitz, Universal jump in the superfluid density of two-dimensional superfluids, Phys. Rev. Lett. **39**, 1201 (1977).
[26] M. E. Fisher and D. R. Nelson, Spin flop, supersolids, and bicritical and tetracritical points, Phys. Rev. Lett. **32**, 1350 (1974).
[27] F. Parisen Toldin, M. Hohenadler, F. F. Assaad, and I. F. Herbut, Fermionic quantum criticality in honeycomb and π-flux Hubbard models: Finite-size scaling of renormalization-group-invariant observables from quantum Monte Carlo, Phys. Rev. B **91**, 165108 (2015).
[28] T. Grover and T. Senthil, Topological spin Hall states, charged skyrmions, and superconductivity in two dimensions, Phys. Rev. Lett. **100**, 156804 (2008).
[29] E. Khalaf, S. Chatterjee, N. Bultinck, M. P. Zaletel, and A. Vishwanath, Charged skyrmions and topological origin of superconductivity in magic-angle graphene, Sci. Adv. **7**, eabf5299 (2021).
[30] M. Christos, S. Sachdev, and M. S. Scheurer, Superconductivity, correlated insulators, and Wess–Zumino–Witten terms in twisted bilayer graphene, Proc. Natl. Acad. Sci. **117**, 29543 (2020).
[31] S. Chakravarty, B. I. Halperin, and D. R. Nelson, Two-dimensional quantum Heisenberg antiferromagnet at low temperatures, Phys. Rev. B **39**, 2344 (1989).
[32] S.-C. Zhang, A unified theory based on SO(5) symmetry of superconductivity and antiferromagnetism, Science **275**, 1089 (1997).
[33] L. E. Hayward, D. G. Hawthorn, R. G. Melko, and S. Sachdev, Angular fluctuations of a multicomponent order describe the pseudogap of $YBa_2Cu_3O_{6+x}$, Science **343**, 1336 (2014).
[34] K. B. Efetov, H. Meier, and C. Pépin, Pseudogap state near a quantum critical point, Nat. Phys. **9**, 442 (2013).
[35] J. M. Kosterlitz, D. R. Nelson, and M. E. Fisher, Bicritical and tetracritical points in anisotropic antiferromagnetic systems, Phys. Rev. B **13**, 412 (1976).
[36] S. Peotta and P. Törmä, Superfluidity in topologically nontrivial flat bands, Nat. Commun. **6**, 8944 (2015).
[37] F. Xie, Z. Song, B. Lian, and B. A. Bernevig, Topology-bounded superfluid weight in twisted bilayer graphene, Phys. Rev. Lett. **124**, 167002 (2020).
[38] R. Sahay, S. Divic, D. E. Parker, T. Soejima, S. Anand, J. Hauschild, M. Aidelsburger, A. Vishwanath, S. Chatterjee, N. Y. Yao, and M. P. Zaletel, Superconductivity in a topological lattice model with strong repulsion, arXiv:2308.10935.
[39] F. F. Assaad, M. Bercx, F. Goth, A. Götz, J. S. Hofmann, E. Huffman, Z. Liu, F. P. Toldin, J. S. E. Portela, and J. Schwab, The ALF (Algorithms for Lattice Fermions) project release 2.0. Documentation for the auxiliary-field quantum Monte Carlo code, SciPost Phys. Codebases 1 (2022).
[40] T. J. Boerner, S. Deems, T. R. Furlani, S. L. Knuth, and J. Towns, Access: Advancing innovation: NSF's advanced cyberinfrastructure coordination ecosystem: Services & support, in *Practice and Experience in Advanced Research Computing*, PEARC '23 (ACM Press, New York, 2023), pp. 173–176.